Journal of Solid State Chemistry 182 (2009) 172–181

Contents lists available at ScienceDirect

Journal of Solid State Chemistry

journal homepage: www.elsevier.com/locate/jssc

# Characterization and thermal stability of cobalt-modified 1-D nanostructured trititanates

Edisson Morgado Jr.[a,*], Bojan A. Marinkovic[b], Paula M. Jardim[b], Marco A.S. de Abreu[a], Fernando C. Rizzo[b]

[a] PETROBRAS S.A./CENPES, Research & Development Centre, Av. Horacio Macedo, 950, Cidade Universitaria, 21941-915 Rio de Janeiro-RJ, Brazil
[b] Department of Materials Science and Metallurgy, Pontifical Catholic University, C.P.: 38008, 22453-900 Rio de Janeiro-RJ, Brazil

ARTICLE INFO

*Article history:*
Received 15 February 2008
Received in revised form
29 September 2008
Accepted 2 October 2008
Available online 18 October 2008

*Keywords:*
Titanate
$TiO_2$
Anatase
1-D nanomaterials
Cobalt
Thermal transformation

ABSTRACT

One-dimensional (1-D) nanostructured sodium trititanates were obtained via alkali hydrothermal method and modified with cobalt via ion exchange at different Co concentrations. The resulting cobalt-modified trititanate nanostructures (Co-TTNS) were characterized by TGA, XRD, TEM/SAED, DRS-UV–Vis and $N_2$ adsorption techniques. Their general chemical formula was estimated as $Na_xCo_{y/2}H_{2-x-y}Ti_3O_7 \cdot {}_{n}H_2O$ and they maintained the same nanostructured and multilayered nature of the sodium precursor, with the growth direction of nanowires and nanotubes along [010]. As a consequence of the $Co^{2+}$ incorporation replacing sodium between trititanate layers, two new diffraction lines became prominent and the interlayer distance was reduced with respect to that of the precursor sodium trititanate. Surface area was slightly increased with cobalt intake whereas pore size distribution was hardly affected. Besides, $Co^{2+}$ incorporation in trititanate crystal structure also resulted in enhanced visible light photon absorption as indicated by a strong band-gap narrowing. Morphological and structural thermal transformations of Co-TTNS started nearly 400 °C in air and the final products after calcination at 800 °C were found to be composed of $TiO_2$-rutile, $CoTiO_3$ and a bronze-like phase with general formula $Na_{2x}Ti_{1-x}Co_xO_2$.



## 1. Introduction

One-dimensional (1-D) nanostructured (nanotubes/nanowires/nanorods) titanates obtained via alkali hydrothermal method [1] can combine large ion exchanging capacity, a typical property of bulk alkaline metal titanates [2,3], with high surface area and mesopore volume [4,5], thus being very promising to catalytic purposes. Sun and Li [6] were the first to study the ion exchangeability of these 1-D nanomaterials and realize the potential use of the corresponding metal-substituted ($Zn^{2+}$, $Cu^{2+}$, $Ni^{2+}$, $Co^{2+}$, $Ag^{+}$ and $Cd^{2+}$) nanotubes after revealing their effects on magnetic and optical properties, while retaining the original morphology of the precursor Na-rich trititanate nanotubes ($Na_{2-x}H_xTi_3O_7 \cdot nH_2O$) without agglomeration of metal particles. This study was followed by researchers considering other elements as the candidates for ion exchange such as alkali metals from $Li^{+}$ to $Cs^{+}$ [7], $Ba^{2+}$ [8], $Ca^{2+}$ [9], $Fe^{3+}$, $Ni^{2+}$ and $Bi^{2+}$ [10], $Au^{2+}/Au^{3+}$, $Pd^{2+}$, $Pt^{2+}$ and $Ru^{3+}$ [11].

Cobalt-modified 1-D nanostructured trititanates obtained via alkali hydrothermal method is of particular interest for photocatalytic application, because apparently they can be excited by visible light [6], unlike their counterparts sodium- or proton-rich trititanate nanotubes/nanowires, which need UV radiation due to their large band-gaps [12]. After the report of Sun and Li about Co-modified trititanate nanotubes and their optical and magnetic properties, there were just few more studies on Co substitution in 1-D trititanate nanomaterials [9,13,14]. Ferreira et al. [9] have submitted $Na^{+}$ enriched nanotubes to ion-exchange reactions replacing sodium by $Co^{2+}$, among other metal cations. While Ferreira et al. [9] observed a significant increase in the interlayer distance for $Co^{2+}$-exchanged nanotubes, Sun and Li [6] reported no apparent change in X-ray diffraction (XRD) pattern after intercalation of $Co^{2+}$ ions between the layers of the multiwalled nanotubes. Sun and Li [6] carried out their ion-exchange reactions by stirring the trititanate nanotubes with the metal salt stabilized in aqueous ammonia solution for 20 h, while the other group [9] simply suspended the nanostructured trititanate powder in the corresponding aqueous solutions of the metal nitrate or chloride for 24 h, both at room temperature. These groups claimed that $Co^{2+}$ substitute for $Na^{+}$ in the interlayers, basically supporting it through XRD, transmission electron microscopy (TEM) and infrared (IR) spectroscopy. On the other hand, Wu et al. [13] and Huang et al. [14] demonstrated that $Co^{2+}$ can also be incorporated in the framework of trititanate nanotubes, at octahedral sites, substituting partially for $Ti^{4+}$. In these two latter cases, a Co-doped anatase ($TiO_2$) was used as the precursor for the alkali

* Corresponding author. Fax: +55 21 3865 6626.
*E-mail address:* emorgado@petrobras.com.br (E. Morgado Jr.).

0022-4596/$ - see front matter © 2008 Elsevier Inc. All rights reserved.
doi:10.1016/j.jssc.2008.10.008

hydrothermal synthesis of trititanate nanotubes with $Co^{2+}$ partially occupying octahedral sites in the framework and found to be weakly ferromagnetic [13,14], as opposed to the trititanate nanotubes containing $Co^{2+}$ within the interlayer position which were reported as antiferromagnetic [6].

Despite the contribution of these studies on the investigation of cobalt-modified trititanate nanotubes, complementary research is needed to fulfill some missing aspects related to the ion-exchange behavior, chemical composition, optical properties, as well as concerned to the effect of the substituted metal ($Co^{2+}$) on the structural and morphological thermal stability of the Co-modified 1-D nanostructured trititanates.

## 2. Experimental

### 2.1. Hydrothermal synthesis of the 1D-trititanate nanostructures (TTNS)

The synthesis was carried out in pilot scale based on previous experiments in laboratory [5]. Commercial nanocrystalline anatase (FINNTi-S140 from Kemira Pigments) of 330 g was mixed to 4650 g of a NaOH (10 M) solution for 5 min under moderate stirring. The alkaline mixture was immediately transferred to a sealed autoclave jacketed for heated oil circulation and equipped with an agitator (helicoidal propeller). Stirring rate was set to 50 rpm and temperature inside the reactor was controlled at $100 \pm 2$ °C for 15 h. After reaction, the circulating oil was cooled down as well as the reactor and the resulting viscous slurry was discharged and diluted with 20 l of deionized water to be filtrated under vacuum. The filter cake was re-suspended in another 20 l of water and filtered again; this latter procedure was repeated twice until practically all unreacted NaOH was removed through the filtrate. The so obtained water-washed precipitate contained approximately 10wt% sodium and was named "Na-TTNS". Part of this sample was submitted to repeated washing/filtration cycles with HCl solution and pH controlled at 1.5 until sodium content was reduced to lower than 1 wt% Na, the resulting sample being finally washed with deionized water for chloride removal and designated as "H-TTNS". Both Na-TTNS and H-TTNS were dried in an air-circulating oven at 120 °C for 15 h to produce the corresponding nanostructured powders.

### 2.2. Synthesis of the cobalt-modified samples (Co-TTNS)

Typically, 5 g of the Na-TTNS sample on dry basis (total amount of water determined by TGA) were added to 250 ml of $Co(NO_3)_2 \cdot 6H_2O$ solution with a pre-established concentration. The suspension was sonicated for 30 min and left under magnetic stirring for 8 h at room temperature ($25 \pm 2$ °C). The colored cobalt exchanged precipitate was then vacuum-filtered, washed with $2 \times 250$ ml of deionized water to remove remaining soluble ions ($Na^+$, $Co^{2+}$ and $NO_3^-$) and dried in air-circulating oven at 120 °C for 15 h to obtain the corresponding cobalt-modified nanostructured powders. Five different initial concentrations of the cobalt nitrate solution were applied: 0.007, 0.017, 0.034, 0.051 and 0.10 mol/liter to produce five Co-TTNS samples namely Co-TTNS/2, Co-TTNS/5, Co-TTNS/10, Co-TTNS/15 and Co-TTNS/30 referring respectively to 2, 5, 10, 15 and 30 wt% of cobalt load, hypothetically assuming complete cobalt incorporation from the exchange solution. This set was designed aiming to establish the saturation point for the metal exchange at 25 °C. The experiment with the most concentrated cobalt solution (0.10 M $Co^{2+}$) was also conducted at 100–110 °C under reflux (Co-TTNS/30R) for 8 h as well.

### 2.3. Heat treatments

The Co-TTNS/30 sample dried at 120 °C was divided into equal portions and heated at 10 °C/min in static air and kept for two hours at the following temperatures: 300, 400, 600 and 800 °C, generating the calcined samples Co-TTNS/300, Co-TTNS/400, Co-TTNS/600 and Co-TTNS/800.

### 2.4. Characterization tools

Sodium and cobalt contents in the solid samples on as-such dried basis (Cs) were determined by atomic absorption spectroscopy (AAS). These metals were not measured in the filtrates after equilibrium; cobalt concentration in the remaining solution (Ceq) was calculated considering the metal adsorbed in the solid subtracted from the amount of cobalt in the starting solution. The percent adsorption of $Co^{2+}$ was calculated as $[(Ci-Ceq)/Ci] * 100$, where Ci is the concentration of cobalt ions in the starting solution. X-ray powder diffraction (XRPD) analyses were performed on a powder diffractometer (Rigaku XRD-6000), operating with Cu$K\alpha$ radiation at 40 kV and 35 mA, step size of 0.02° $2\theta$ and step time of 5 s. All samples for XRPD were prepared using the classical procedure by mixing always the same amount of powder with isopropyl alcohol within the sample holder. Precise determination of $d$-values related to interlayer spacing via single-line fitting was performed using the software Topas-Academic, which was also applied for quantitative phase analysis of XRPD patterns by Rietveld method of the samples thermally treated at 600 and 800 °C. TEM images and selected area electron diffraction (SAED) were recorded using a Gatan CCD camera on a JEOL-2010 microscope operating at 200 kV. Specimens for TEM observation were prepared by dispersing the powder in alcohol by ultrasonic treatment, then dropping onto a holey carbon film supported by a copper grid. Thermogravimetric (TG) measurements were performed in a Shimadzu TGA51-H under dry air flow (50 ml/min); temperature range was 25–800 °C with a heating-up rate of 5 °C/min. Diffuse-reflectance UV–Vis spectra (200–800 nm) of the samples pre-treated at 120 °C/12 h were acquired at room temperature in a spectrometer Perkin-Elmer Lambda 900, using $\alpha$-$Al_2O_3$ as reflectance reference. UV–Vis absorption was expressed as the Kubelka–Munk function—$F(R)$. Assumed an indirect transition for the fundamental absorption [15], the apparent band-gap energies were obtained by plotting $(F(R)h\upsilon)^{1/2}$ against $h\upsilon$ (photon energy) and extrapolating the straight line portion of the UV–Vis spectra to $(F(R)h\upsilon)^{1/2} = 0$ [16]. Textural properties of the powder samples, pretreated at 120 °C under vacuum down to 50 mTorr, were characterized by $N_2$ adsorption at −196 °C on a Micromeritics TriStar 3000 V6.03 instrument. Specific surface area was calculated by using the classic BET equation in the $P$/Po range of 0.06–0.21, and the pore volume distribution within the 2–60 nm diameter range was determined by means of the Barrett–Joyner–Halenda (BJH) algorithm method using the adsorption branch of the isotherm (the desorption branch was avoided due to an artifact peak in the pore distribution caused by the tensile strength effect [5,17]).

## 3. Results and discussion

### 3.1. Cobalt exchange behavior

In preliminary experiments, the proton exchanged support (H-TTNS) revealed difficult exchangeability with cobalt ions and no more than 0.5 wt% cobalt could be retained in the solid material. Therefore, our efforts concentrated on the water washed

material Na-TTNS, which demonstrated easy exchange capacity with cobalt. The calculated weight percentage of cobalt for each Co-TTNS sample is listed in Table 1; one can notice that measured and nominal cobalt content (based on the total amount of cobalt ions) were similar to each other up to 5 wt% Co, indicating full absorption of cobalt ions from the starting solution, as the colorless filtrates also suggested. That is also demonstrated in Fig. 1a, where the percent adsorption for $Co^{2+}$ (as defined in Section 2.4) is plotted as a function of the concentration of the starting solution. The initial complete sorption gave way to an exponential decrease of cobalt sorption at higher adsorbate concentrations, suggesting a trend of saturation.

The cobalt ion-exchange isotherm is presented in Fig. 1b. The isotherm profile was rather fitted to the classical adsorption models: Freundlich ($R^2 = 0.81$) and Langmuir model ($R^2 = 0.79$). The limited number of experimental points did not encourage us to look into the cobalt exchanging kinetics, which was not the aim of this investigation.

**Table 1**
AAS and TG results used to calculate the chemical formulae of the samples studied and their corresponding band-gap energies estimated from the plot in Fig. 5a

| Sample | wt% Na A.A.S. | wt% Co A.A.S. | wt% loss (30–100 °C) | wt% loss (100–500 °C) | Formula | Band-gap energy (eV) |
|---|---|---|---|---|---|---|
| Na-TTNS | 10.6 | 0.0 | 6.8 | 8.6 | $Na_{1.57}H_{0.43}\ Ti_3O_7 \cdot 1.41H_2O$ | 3.50 |
| Co-TTNS/2 | 6.78 | 1.99 | 9.4 | 8.4 | $Na_{1.00}Co_{0.12}H_{0.76}\ Ti_3O_7 \cdot 1.20H_2O$ | 2.70 |
| Co-TTNS/5 | 5.00 | 4.97 | 8.7 | 8.5 | $Na_{0.75}Co_{0.31}H_{0.64}Ti_3O_7 \cdot 1.31H_2O$ | 2.55 |
| Co-TTNS/10 | 1.94 | 9.11 | 8.8 | 8.6 | $Na_{0.29}Co_{0.54}H_{0.63}Ti_3O_7 \cdot 1.36H_2O$ | 2.56 |
| Co-TTNS/15 | 1.35 | 9.32 | 8.7 | 8.6 | $Na_{0.20}Co_{0.55}H_{0.70}Ti_3O_7 \cdot 1.31H_2O$ | 2.55 |
| Co-TTNS/30 | 1.04 | 10.9 | 9.3 | 8.4 | $Na_{0.16}Co_{0.66}H_{0.52}Ti_3O_7 \cdot 1.42H_2O$[a] | 2.55 |
| Co-TTNS/30R | 1.06 | 10.4 | – | – | – | – |
| H-TTNS | 0.99 | 0.0 | 7.1 | 7.8 | $Na_{0.12}H_{1.88}\ Ti_3O_7 \cdot 0.30H_2O$ | 3.38 |

[a] Formula of Co-TTNS/30 may not be strictly correct due to the presence of anatase impurity.

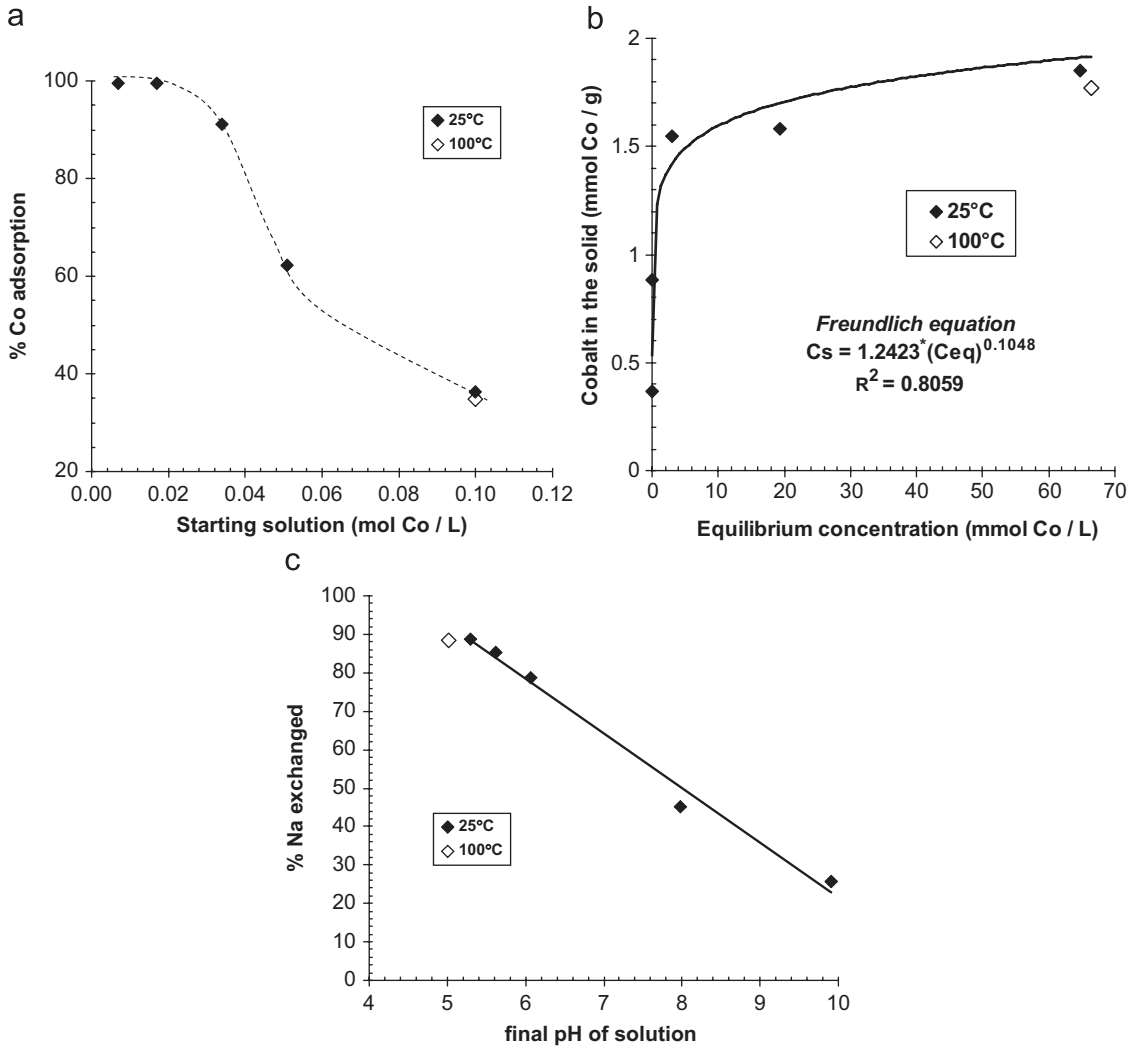


**Fig. 1.** (a) Adsorption percentage of cobalt from solution by Na-TTNS as a function of the starting solution concentration: $m = 5$ g, $V = 250$ ml, time 8 h; (b) Freundlich fitted adsorption isotherm for $Co^{2+}$ on the TTNS material; (c) percentage of sodium removed from Na-TTNS as a function of the measured pH of the cobalt solutions.

As given in Table 1, the amount of exchanged cobalt was accompanied by the corresponding loss of sodium from the solid. However, the maximum exchange of cobalt has not resulted in complete sodium removal; nearly 10% of the total sodium remained in the solid indicating the existence of inaccessible sodium sites difficult to be reached and exchanged. It is important to note (Fig. 1a and b; Table 1) that working at higher temperature (reflux at ~100 °C) has not changed the maximum amount of exchangeable cobalt in the solid neither the percentage of residual sodium. Cobalt ions in excess may not be the only driving force for the sodium exchange. As the concentration of the initial solution increased, pH of the solution dropped due to hydrolysis of the cobalt salt thus generating protons that might be also involved in the process as suggests the correlation in Fig. 1c.

### 3.2. Morphological and crystallographic properties

The as-synthesized samples with different Co contents maintained the original 1-D morphology of the precursor Na-rich nanostructure, appearing predominantly as multilayered malformed nanowires aligned or randomly distributed (Fig. 2a and b), while nanotubes are hardly observed. Extra TEM images are provided as supplemental data for visual proof of the morphological features described in this section. The growth direction of the nanowires is along [010] direction, as indicated by electron diffraction (inset in Fig. 2a). This is consistent with our earlier studies [4,5,8,12,18] of growth direction in trititanate 1-D nanomaterials obtained via alkali hydrothermal route and previously identified [4,6,9,15] as monoclinic $Na_{2-x}H_xTi_3O_7 \cdot nH_2O$ with the crystal structure corresponding to the structure of the compounds $Na_2Ti_3O_7$ (ICSD: 15463) or $D_2Ti_3O_7$ (ICSD: 41055). Therefore, our experimental findings cannot support the systematization of growth directions in such materials as given by Bavykin et al. [19], suggesting that nanowires, directly obtained through this route, grow along [001] direction. Bavykin et al. based their definition of growth direction in trititanate nanowires on the results earlier reported by Yang and Zheng [20]. Another characteristic of the as-synthesized Co-TTNS materials is that cobalt is exclusively associated to these nanostructures, as it is exemplified through a selected EDS spectrum (Fig. 2c), so that no kind of Co segregation in the form of oxide or metallic nanoparticles could be found in the analyzed samples.

After a meticulous examination by TEM/SAED, it was verified that both Co-TTNS/30 and Co-TTNS/30R were the only specimens exhibiting some segregated non-layered particles with anatase structure as illustrated in Fig. 2d. The picture suggests that these nanoparticles arise from the 1-D nanostructured titanates. These

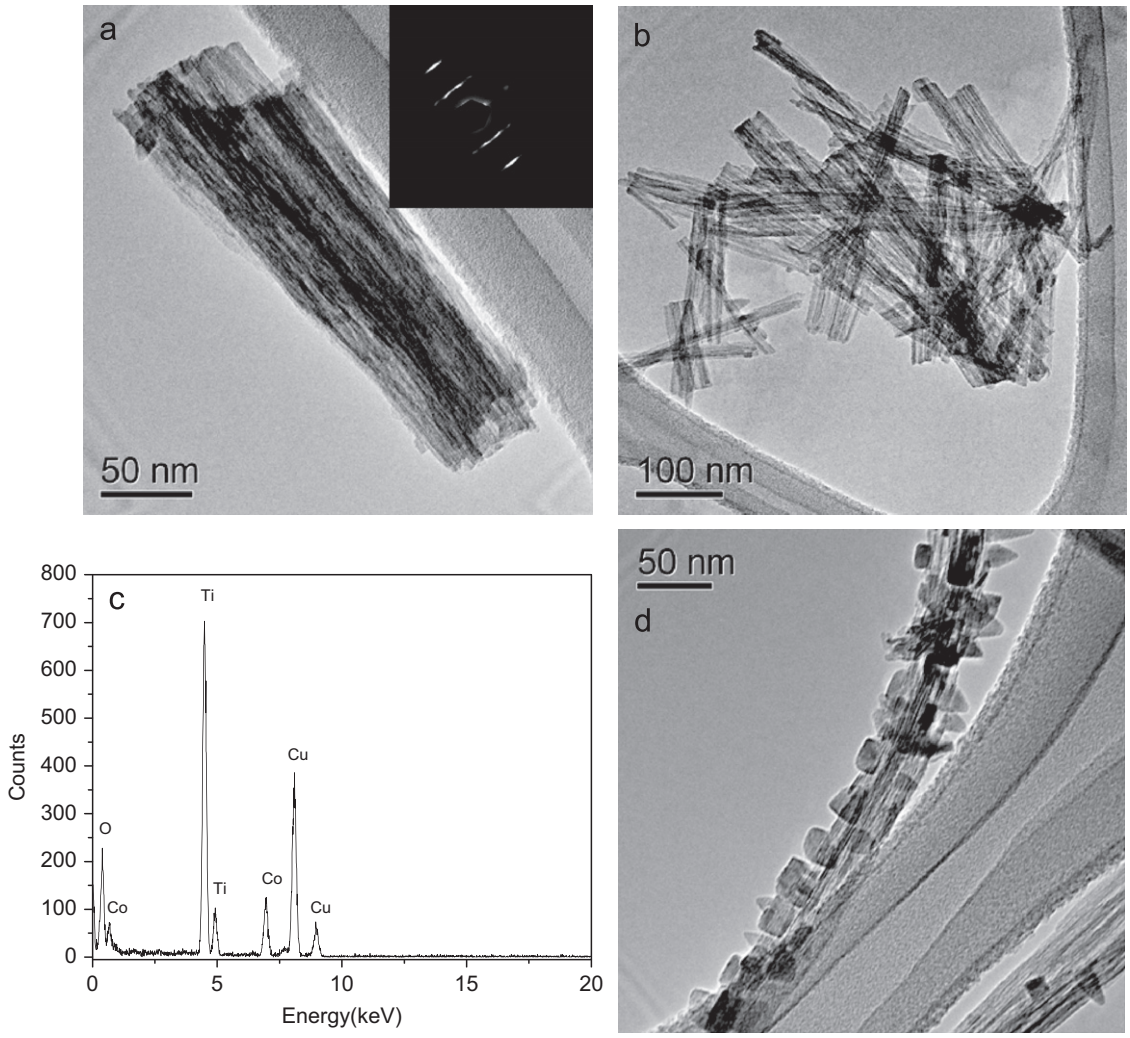


**Fig. 2.** (a) TEM image and SADP from the sample Co-TTNS/30 of a bundle of aligned trititanate 1-D nanostructures; (b) TEM image showing randomly distributed 1-D nanostructures and (c) the corresponding EDS spectrum; (d) TEM image of the sample Co-TTNS/30 showing trititanate 1-D nanoparticles with deposited anatase nanoparticles.

two samples underwent the exchange condition with the highest concentration of cobalt salt in solution thus resulting in the lowest pH (Fig. 1c). It is already known in literature that transformation of nanostructured titanates into $TiO_2$ polymorphs tend to occur under acidic pH environment [21–23]. Therefore, one could conclude that a small part of the 1-D trititanate was converted into $TiO_2$-anatase during cobalt exchange at this condition. The high excess of cobalt in the exchanging solution should be avoided if transformation of TTNS into anatase nanoparticles is undesired.

XRD patterns of the as-synthesized specimens (Fig. 3) revealed four typical diffraction lines of trititanate 1-D nanomaterials situated at around 10°, 24°, 28° and 48° $2\theta$ (Cu$K\alpha$) accompanied with two new lines emerging at ~34° and 40° $2\theta$ (Cu$K\alpha$). These two latter lines seem to be a peculiar feature of the $Co^{2+}$-exchanged 1-D titanate nanomaterials, since they are not prominent in the sodium precursor (Na-TTNS), while in the proton derived specimen (H-TTNS) these peaks cannot be observed at all (Fig. 3). It can be noticed as well that the intensities of these two lines increase gradually with the increase of cobalt exchanged in the 1-D nanomaterial (compare, for instance, XRPD patterns of Co-TTNS/2 and Co-TTNS/30). An influence of preferential orientation on the appearance of these two peaks can be excluded since all the samples (as-synthesized and Co-exchanged) were prepared on the same manner for XRPD measurements, as described in the experimental section. These two extra lines have also been observed in the XRD pattern of Co-modified trititanate nanotubes prepared by Ferreira et al. [9], who found by IR spectroscopy that $Co^{2+}$ is incorporated between the layers of trititanate structure and not in the layer structure built of $(Ti_3O_7)^{2-}$ framework.

The partial formation of anatase particles as observed by TEM exclusively in the samples Co-TTNS/30 and Co-TTNS/30R was hardly detected by XRD, possibly due to a combination of three

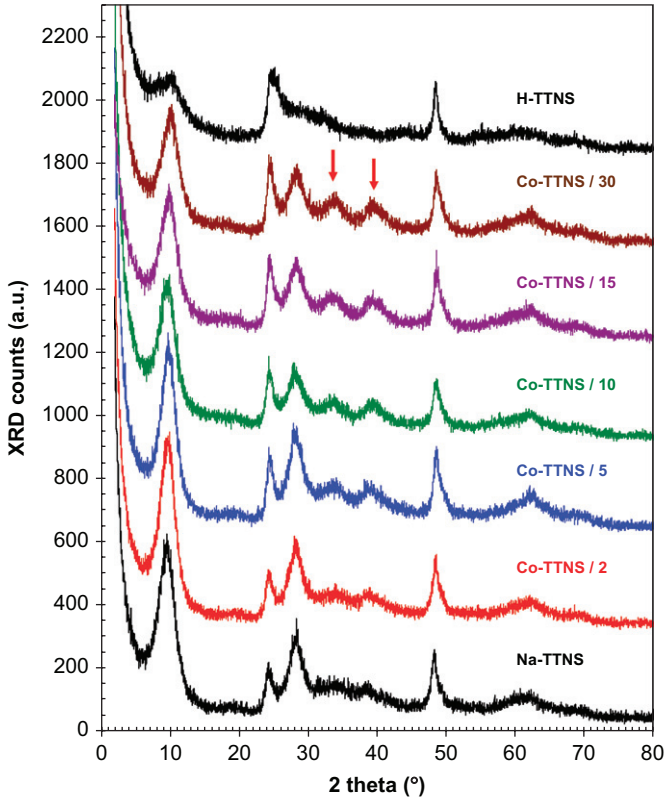


**Fig. 3.** XRPD patterns of as-synthesized samples (see Table 1 for sample description). The arrows indicate two diffraction lines fingerprints of Co insertion within trititanate interlayers.

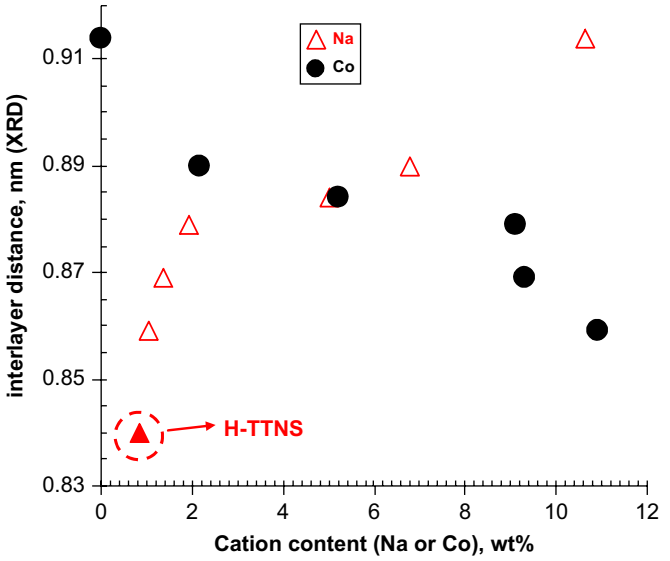


**Fig. 4.** Interlayer distance measured by XRPD as a function of the exchanged cobalt (sodium) content. The measurement for H-TTNS with low sodium content is also plotted as reference.

factors: (i) small quantity, (ii) nanosize and (iii) main diffraction line ($2\theta = 25.2°$) very close to that of the dominant 1-D trititanate phase ($2\theta = 24.5°$). For the rest of the Co-TTNS samples, XRD confirmed TEM findings in that they are single-phased, composed just of trititanate phase.

An examination of the XRD patterns in Fig. 3 by single-line fitting also reveals that the first diffraction line (related to the interlayer spacing) is shifted to higher $2\theta$ values when cobalt substitutes for sodium. As displayed in Fig. 4, the $d$-value is reduced upon increasing the amount of cobalt exchanged. Such shrinkage of the lamellar structure may be directly ascribed to the incorporation of cobalt since its ionic radius at any coordination number is significantly smaller than the ionic radius of sodium in the lattice [24]. Comparatively, a larger reduction in the interlayer distance takes place when the same amount of sodium is replaced by proton (see H-TTNS data point in Fig. 4); however, the mechanism of reduction in interlayer spacing after proton exchange is mainly explained by removal of interlayer water as earlier demonstrated [4,5]. It is worth mentioning that it was not possible to measure accurately the intershell spacing through HRTEM images due to significant variations of this distance along the nanowires axis, and for this reason they were not compared to those determined by XRD data. Besides, the latter is much more representative of the average values of all 1-D titanate crystals contained in the samples, whereas the interlayer distances obtained from TEM images might be misleading since they are based on relatively few measurements.

### 3.3. Thermal analyses and chemical composition

As previously observed in TG experiments of 1-D nanostructured titanates [4,5], water is also released up to 500 °C in Co-TTNS specimens. Approximately half of this water is lost at temperatures lower than 100 °C, which is due to physically adsorbed water and not relevant for determination of the chemical formulae of the nanostructured trititanates. All Co-exchanged samples exhibited a very similar percentage of weight loss between 100 and 500 °C, as much as their sodium precursor (Table 1). From earlier studies with TTNS samples it could be established [4,5,18] that water loss at lower temperatures

(100–200 °C) is mostly due to interlayer water ($H_2O$) while the water lost over 200–500 °C range is mainly structural water (−OH). Based on the water loss between 100 and 500 °C, estimated from TG results, and the weight percentages of Co and Na obtained from AAS one can calculate chemical formulae of Co-modified trititanate 1-D nanostructures (Table 1) following the methodology described in Appendix A and previously used for the calculation of chemical formulae of Na- and H-rich trititanate nanotubes [4,5,12,18]. From the estimated chemical formulae (Table 1) it can be observed that sodium content decreased with the increase of cobalt content as expected based on the results described in Section 3.1. The amount of Interlayer water (expressed as $n$, where $n$ is the number of interlayer water molecules per chemical formula) did not change significantly with $Co^{2+}$ substitution if compared to the interlayer $H_2O$ content in its precursor Na-TTNS, thus clearly contrasting with the dehydration promoted by the proton exchange (H-TTNS). This finding hence suggests that the reduction of $d$-values of interlayer distances in $Na_xCo_{y/2}H_{2-x-y}Ti_3O_7 \cdot nH_2O$ with the increase in cobalt content as verified in Fig. 4, is majorly related to the entrance of smaller $Co^{2+}$ in the interlayers substituting larger $Na^+$. Another evidence in favor of the cobalt exchange with interlayer sodium is that H in the formulae of all Co-exchanged samples remained rather constant and not much higher than that found in the formula of the Na-TTNS (water washed precursor). Finally, it should be pointed out that strictly speaking, the formula ascribed to the Co-TTNS/30 specimen in Table 1 may not be correct due to the conversion of a minor portion of the 1D-trititanate into anatase nanoparticles.

### 3.4. Optical properties

The optical absorption spectra are depicted in Fig. 5 with all samples exhibiting a fundamental absorption at short wavelength. However, optical properties of Co-exchange trititanate 1-D nanomaterials are rather different from that observed for Na- and proton-rich 1-D nanomaterials. A strong red-shift of the absorption edge for Co-exchanged 1-D nanomaterials is verified even for the lowest content of ionic exchange (see curve of Co-TTNS/2 specimen in Fig. 5a and Table 1). The calculated band-gap (2.70 eV) is shifted ~0.80 and 0.68 eV relative to the band-gaps of the corresponding sodium- and proton-rich materials, respectively. This red-shift becomes more pronounced for higher Co contents as graphically estimated from Fig. 5a (Table 1), with band-gaps of these samples situated around 2.55 eV thus resulting in red-shifts of 0.95 and 0.83 eV relative to the Na-TTNS and H-TTNS counterparts. There are several experimental and theoretical evidences regarding the influence of transition metals or substitutional doping with N, S, P, C and F on the band-gap narrowing of wide gap semiconductors, such as $TiO_2$ (anatase or rutile), ZnO and $H_2Ti_3O_7$ [10,15,25–30]. A theoretical study conducted by Nishikawa et al. [26] on $TiO_2$ band-gap narrowing after introduction of transition metals explained this effect through the insertion of the metal 3$d$ orbitals within the forbidden band and their interaction with the oxygen 2$p$ orbitals from the valence band, thus leading to decreased band-gap energies. Among other authors, Anpo et al. [25] and Wang et al. [27] observed experimentally for $TiO_2$ similar band-gap narrowing behavior as a consequence of transition metal doping. In the case of substitutional doping with N or C it is supposed that 2$p$ orbitals of these elements are mixing with 2$p$ orbitals of oxygen, also resulting in a reduction of the band-gap values [28]. Wu et al. [29] showed that C substitutional doping strongly reduces band-gap in $TiO_2$ and that this reduction is sensitive to the percentage of C doping, being more pronounced for higher substitution levels.

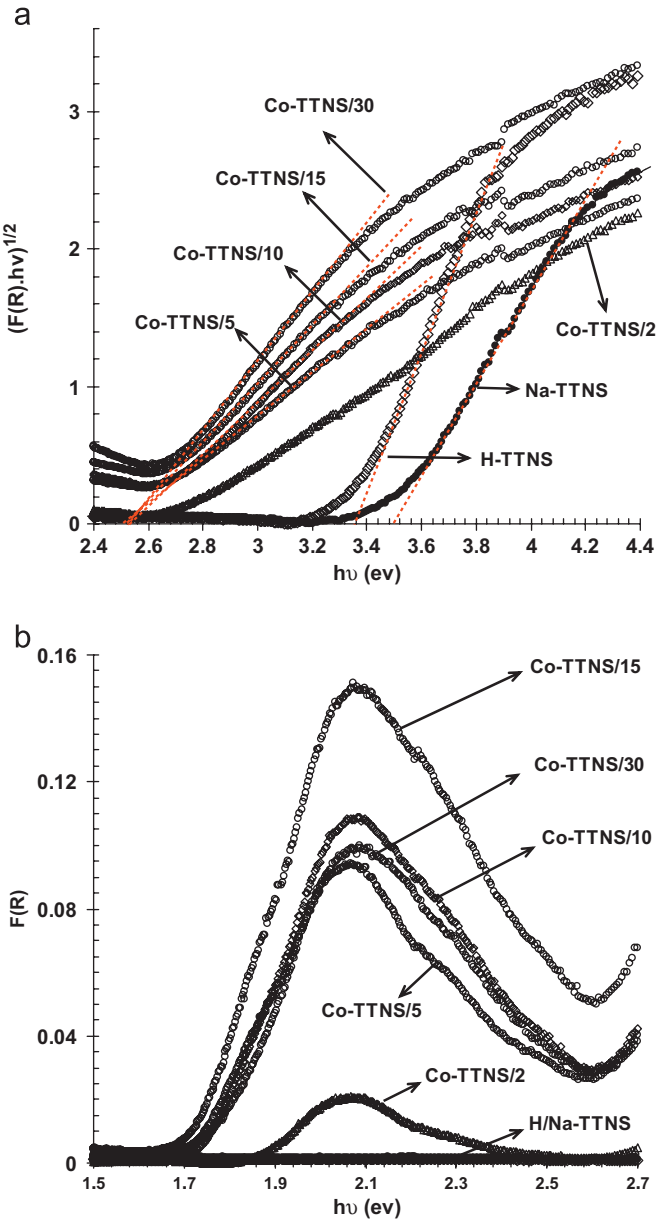


**Fig. 5.** (a) Variation of $(F(R)h\upsilon)^{1/2}$ as a function of excitation energy and the extrapolations ($(F(R)h\upsilon)^{1/2} = 0$) used to obtain the apparent band-gap energies of the as-synthesized TTNS samples with different Co contents and their Na-TTNS and H-TTNS references; (b) UV–Vis spectra within the region 1.5–2.7 eV.

Similar feature for $Fe^{3+}$ doping in $TiO_2$ was noticed by Choi et al. [30]. For trititanate 1-D nanostructures it was already experimentally observed by Peng et al. [10] that doping with transition metals ($Fe^{3+}$ and $Ni^{2+}$) reduces the band-gap. Peng et al. [15] also reported a theoretical study about the effect of $Fe^{3+}$ doping on the band-gap of 1-D trititanates, confirming the red-shift experimentally observed. As occurred in these cases, the strong band-gap narrowing in our Co-exchanged trititanate 1-D nanostructures is likely attributed to the insertion of the $Co^{2+}$ 3$d$ orbitals within the forbidden band. This is another indication that $Co^{2+}$ ions are not segregated as separate particles at the surface of trititanate 1-D nanostructures, but actually incorporated in the trititanate structure within interlayers, forming compounds with the general formula of $Na_xCo_{y/2}H_{2-x-y}Ti_3O_7 \cdot nH_2O$.

As displayed in Fig. 5b, the UV–Vis spectra of Co-modified 1-D nanomaterials also exhibit a hump at around 2.6–1.7 eV

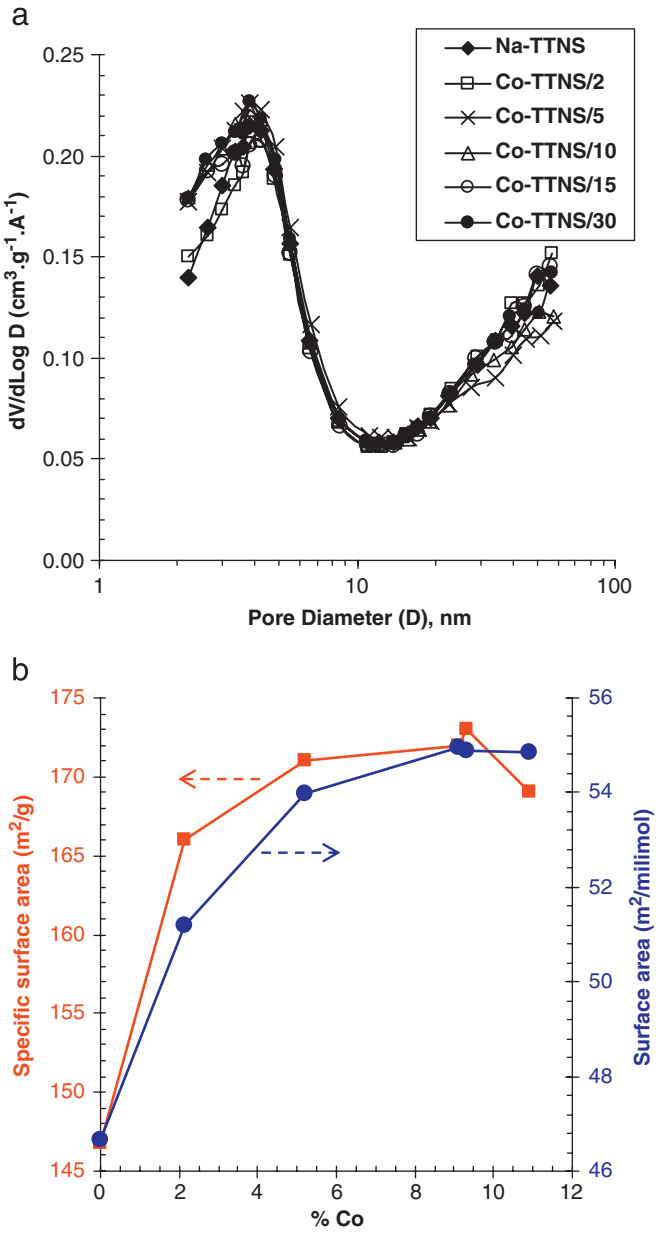


**Fig. 6.** (a) Pore volume distribution (BJH desorption) of Co-TTNS specimens and their Na-TTNS precursor; (b) specific surface area (BET) and the same normalized on molar basis (BET multiplied by Mol) as a function of cobalt content.

($\lambda = 480$–$730$ nm), typical of *d*–*d* transitions as previously identified by Sun and Li [6]. The absorption band due to *d*–*d* transition is a common feature for the semiconductors doped with transition metals [10,31]. As Na-TTNS or H-TTNS are semiconductors, it can be speculated that introduction in the trititanate structure of $Co^{2+}$ *d* states results in their splitting under the influence of the crystal field, leading to the formation of lower and higher *d* energy states, as similarly occurred for $Ni^{2+}$-doped trititanates [10]. Such assumption is supported by the increase in the intensity of this *d*–*d* transition with the amount of exchanged cobalt as evident in Fig. 5b. However, it suffers a discontinuity with the sample Co-TTNS/30 showing a significant reduction in the band intensity when compared to that of Co-TTNS/15 and becoming comparable to that of sample Co-TTNS/10. The only explanation found for such anomalous behavior was a bulk dilution effect provoked by the formation of some anatase as described in Section 3.2 for this particular sample.

From the practical point of view, our experimental results demonstrated that Co-modified trititanate 1-D nanomaterials have improved visible light photon absorption efficiency as compared to their Na- and proton-rich counterparts.

### 3.5. Textural properties

As observed in Fig. 6a, the Co-exchanged samples exhibited a typical pore volume distribution with two main contributions [5]. Pores smaller than 5 nm may be attributed to the inner space of existent nanotubes and may be also due to the small pores created between aligned nanowires/nanorods (Fig. 2a). Larger mesopores likely account for intercrystallite voids generated from the aggregation of the 1-D nanoparticles or also between their small agglomerates. Compared to the precursor Na-TTNS, the gradual incorporation of cobalt did not modify significantly the pore distribution profile, corroborating the TEM observations, which showed no apparent change in the nanoparticles morphology after cobalt exchange.

On the other hand, as previously reported by Sun and Li [6], a measurable increase in surface area was observed with the replacement of sodium by cobalt, either on weight or on molar basis (Fig. 6b). However, this increase in specific surface area of nearly 15% ($147 \rightarrow 170\ m^2/g$) is rather modest if compared to the strong effect of protonation; H-TTNS resulted in twice as much BET surface area ($308\ m^2/g$) confirming earlier findings [4,5]. The increase in surface area occurred up to the point where cobalt exchange nearly saturated. Such small effect may be partly attributed to the contraction of the interlayer space, as previously hypothesized on protonation of sodium rich 1D nanostructured trititanates [5].

### 3.6. Thermal stability

Morphological and crystal structure thermal stabilities of trititanate 1-D nanostructures modified with the highest cobalt content (Co-TTNS/30) were studied by XRPD and TEM. Crystal structure stability is maintained up to 400 °C as can be inferred from XRPD patterns (Fig. 7). However, TEM and EDS (X-ray energy

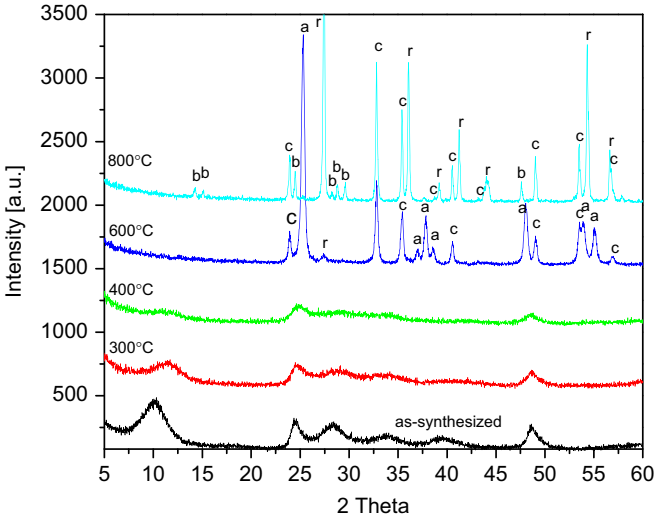


**Fig. 7.** XRPD patterns of sample Co-TTNS/30 as-synthesized and after heat-treatment at 300, 400, 600 and 800 °C (*a* = anatase, *b* = $TiO_2$(B)/bronze, *c* = $CoTiO_3$, *r* = rutile).

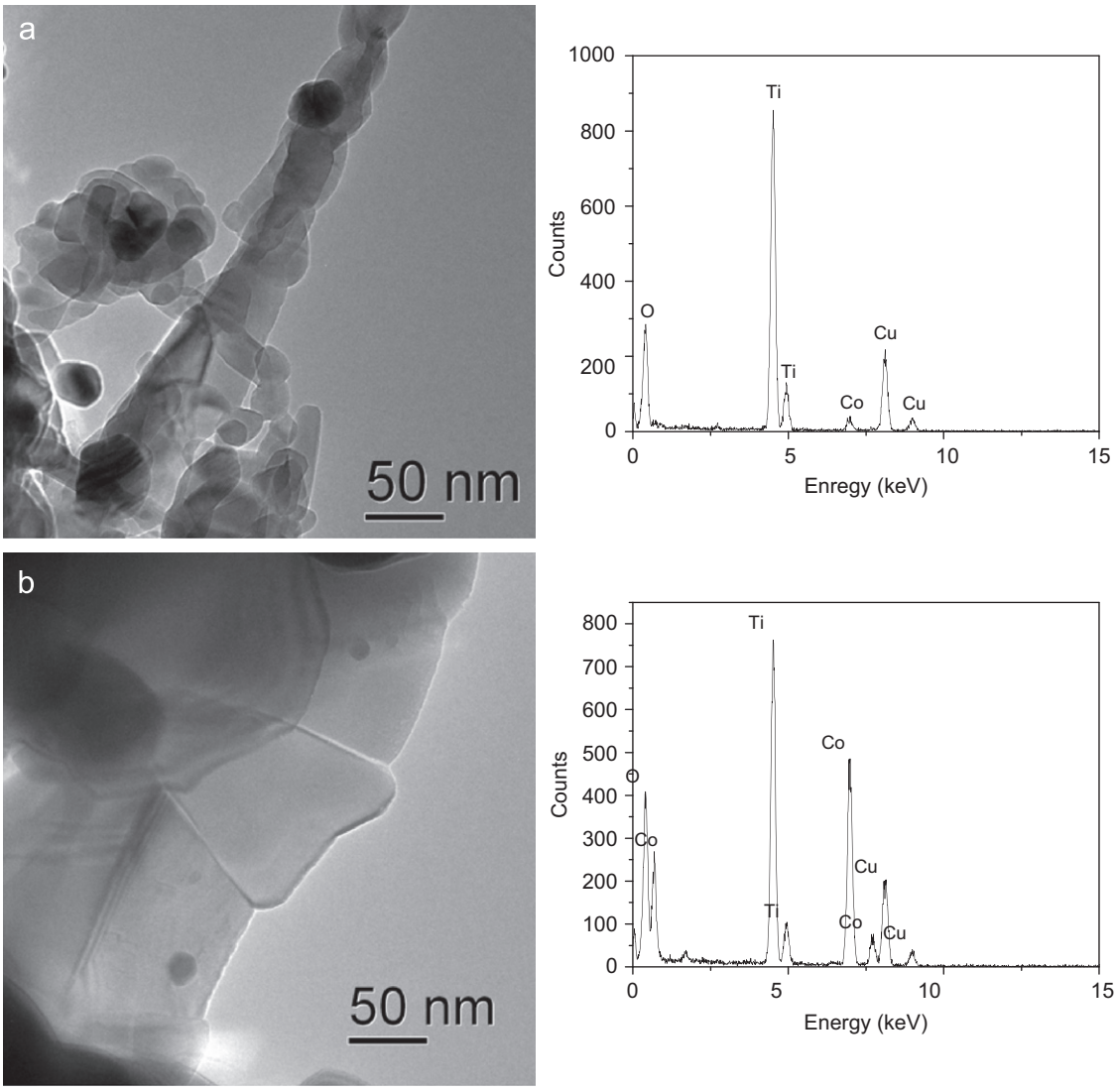


**Fig. 8.** TEM images and corresponding EDS spectra of sample Co-TTNS/30 heat-treated at 400 °C showing the presence of anatase (a) and $CoTiO_3$ (b) nanoparticles.

**Table 2**
Weight percentage of the crystal phases, estimated by Rietveld method, present in the sample Co-TTNS/30 calcined at 600 and 800 °C

| Sample/crystal phase | Anatase (wt%) | $CoTiO_3$ (wt%) | Rutile (wt%) | $TiO_2$(B)/bronze (wt%) |
|---|---|---|---|---|
| Co-TTNS/600 °C | 64.5 | 31.2 | 4.3 | – |
| Co-TTNS/800 °C | – | 28.4 | 59 | 12.6 |

dispersive spectroscopy) observations (Fig. 8a and b) indicated that some nanoparticles of $TiO_2$-anatase and $CoTiO_3$ can be already detected at 400 °C (together with predominant 1-D nanostructured trititanate), meaning that the onset of morphological and crystal structure instability is situated around 400 °C. It is worth citing for comparison our previous work [18] where thermal stability of protonated and sodium rich 1-D trititanates were evaluated and found to be at about 300 and 600 °C, respectively. That means that Co-exchanged 1-D trititanates possess an intermediate thermal stability, which also indicates that cobalt was inserted into the TTNS structure to cause such an effect.

At 600 °C no trace of trititanate crystal structure and 1-D morphology could be found as demonstrated in Figs. 7 and 9a, respectively. Table 2 summarizes the weight percentage of the crystal phases presented at 600 and 800 °C, estimated by Rietveld method. The sample treated at 600 °C contained mostly anatase and $CoTiO_3$ and some rutile, which was confirmed by TEM. However, some $TiO_2$(B) crystals displayed in Fig. 9b were also identified by high-resolution transmission electron microscopy (HRTEM), even though not evident in XRPD pattern taken from the sample treated at 600 °C (Fig. 7). From TEM examination it was clear that at 600 °C the crystal domains of $TiO_2$(B) were rare and when encountered they were very small (~10 nm) and found

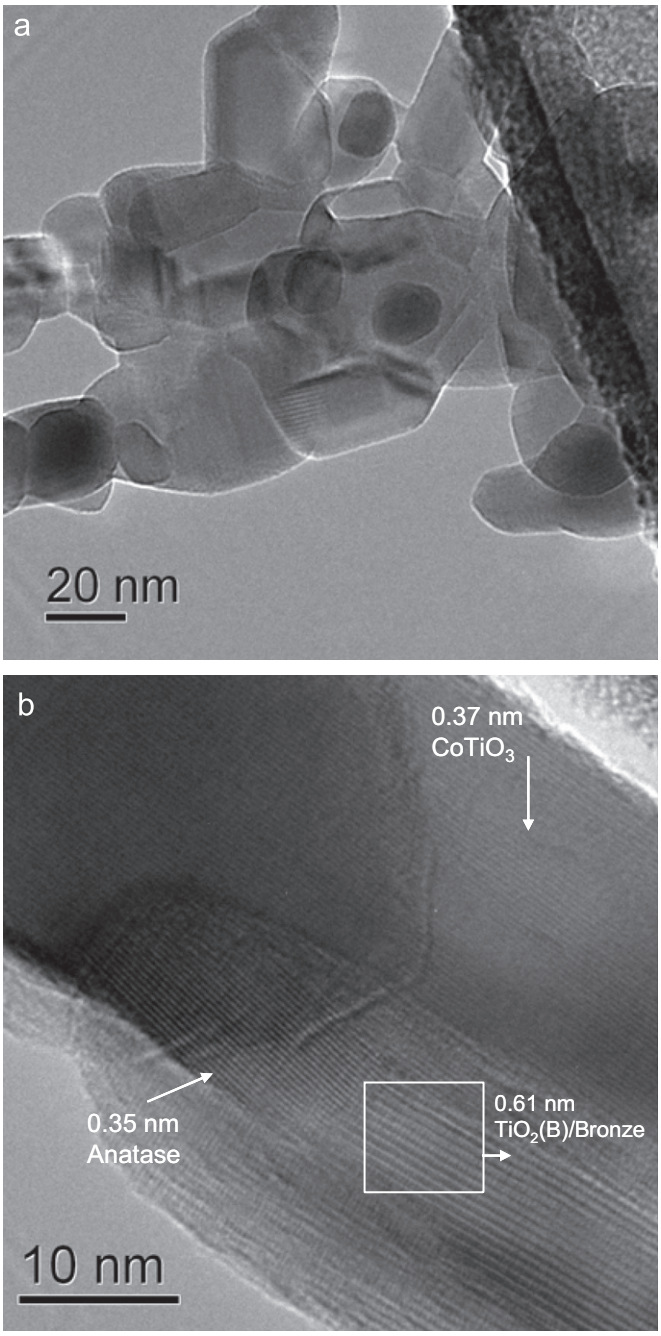


**Fig. 9.** (a) TEM image of sample Co-TTNS/30 heat-treated at 600 °C. (b) Anatase ($d(101) = 0.35$ nm), $CoTiO_3$ ($d(021) = 0.37$ nm) and $TiO_2$(B) ($d(001) = 0.61$ nm) identified by the lattice fringes in the HRTEM image.

between anatase and $CoTiO_3$ phases (Fig. 9b). The small quantity and small size of these domains should result in broad, low intensity diffraction lines, which in practice are not visible in our XRD patterns. Because of the appearance of $TiO_2$(B) as very small nanocrystals closely associated with anatase and $CoTiO_3$ phases it was not possible to evaluate their EDS signal without interference of signals from neighbor anatase and $CoTiO_3$ nanocrystals.

XRPD of the sample treated at 800 °C showed, on the other hand, $TiO_2$(B) together with rutile and $CoTiO_3$ (Fig. 7 and Table 2). Anatase, the predominant phase at 600 °C, was absent at 800 °C. The existence of metastable $TiO_2$(B) phase is totally unexpected at this temperature, since $TiO_2$(B) is often the very first $TiO_2$ phase to be formed (at about 400 °C) after the decomposition of protonated trititanates, serving as the precursor for the formation of anatase at around 500 °C [4,5,12]. The presence of $TiO_2$(B)-like nanocrystals at 800 °C was confirmed by TEM (Fig. 10a and b). However, EDS of these nanocrystals (Fig. 10c) showed that some Na and Co were also associated with them so that the stabilization of the $TiO_2$(B) structure by forming a kind of bronze with $Co^{2+}$ and $Na^+$ ions has been considered. Bronze ($Na_xTi_{1-x}O_2$) and $TiO_2$(B) phases have the same host framework [32] (a very good fit of the diffraction lines from the XRPD pattern taken at 800 °C that do not belong to $TiO_2$-rutile and $CoTiO_3$ can be obtained assuming either $TiO_2$(B) or $Na_xTi_{1-x}O_2$ as structural model). However, differently from $TiO_2$(B) phase, bronze is synthesized under reduction conditions with $Ti^{4+}$ partially reduced to $Ti^{3+}$. As the heat treatment at 800 °C was carried out in air, the appearance of bronze cannot be easily explained through the reduction of $Ti^{4+}$ to $Ti^{3+}$. Nonetheless, there were some evidences in favor of the bronze phase formation. The $CoTiO_3$ is slightly consumed (~31% → ~28%; Table 2) when the sample is heated from 600 to 800 °C and $TiO_2$(B)-like nanocrystals are observed at 600 °C (Fig. 7b), indicating that such phase is formed in the regions between $CoTiO_3$ and anatase and hence strengthening the role of the $CoTiO_3$ partial decomposition in the formation of a bronze-like phase. These observations together with EDS results (showing that Co is associated with bronze nanocrystals, Fig. 10c) suggest that the formation of bronze-like phase is possible in air at 800 °C through the partial incorporation of $Co^{2+}$ (originated from the $CoTiO_3$ decomposition) in the octahedral $Ti^{4+}$ sites, forming bronze-like structures with general chemical formula $Na_{2x}Ti_{1-x}Co_xO_2$. As such bronze structure possess the same host framework as that of $TiO_2$(B), both phases cannot be unequivocally distinguished in our XRPD.

By comparing thermal stability and phase transformation path of Co-rich trititanates as described in the present paper with those with $Na_xH_{2-x}Ti_3O_7 \cdot nH_2O$ formula as previously reported [4], the differences are evident, demonstrating that phase transformation path of TTNS is affected by the presence of cobalt.

## 4. Conclusions

Co-modified trititanate 1-D nanostructures with the general chemical formula $Na_xCo_{y/2}H_{2-x-y}Ti_3O_7 \cdot nH_2O$ have been prepared through ion-exchange of hydrothermally synthesized Na-rich trititanates. The cobalt exchange capacity was established as well as the appropriate exchanging condition to avoid conversion of the 1-D nanostructured layered titanates into anatase nanoparticles.

It is observed that the growth direction of Co-modified nanowires/nanotubes is along [010]. Two diffraction lines at 34° and 40° (Cu$K\alpha$) are an indication of $Co^{2+}$ incorporation in the interlayer sites of trititanate structure. As an effect of $Co^{2+}$ incorporation between trititanate layers, the interlayer distance is reduced with respect to that of the precursor sodium trititanate. This effect is due to the entrance of smaller $Co^{2+}$ ions in the interlayers. Surface area is slightly increased up to the exchange saturation point whereas pore size distribution is hardly affected.

$Co^{2+}$ incorporation in trititanate crystal structure also results in enhanced visible light photon absorption efficiency due to a strong band-gap narrowing.

The onset of morphological and structural thermal instability of Co-modified trititanate 1-D nanostructures is situated around 400 °C. The appearance of bronze-like phase at 800 °C in air is possible through the incorporation of $Co^{2+}$, generated from partial decomposition of $CoTiO_3$, in the octahedral sites originally occupied by $Ti^{4+}$ and then forming nanocrystals with the general formula $Na_{2x}Ti_{1-x}Co_xO_2$.

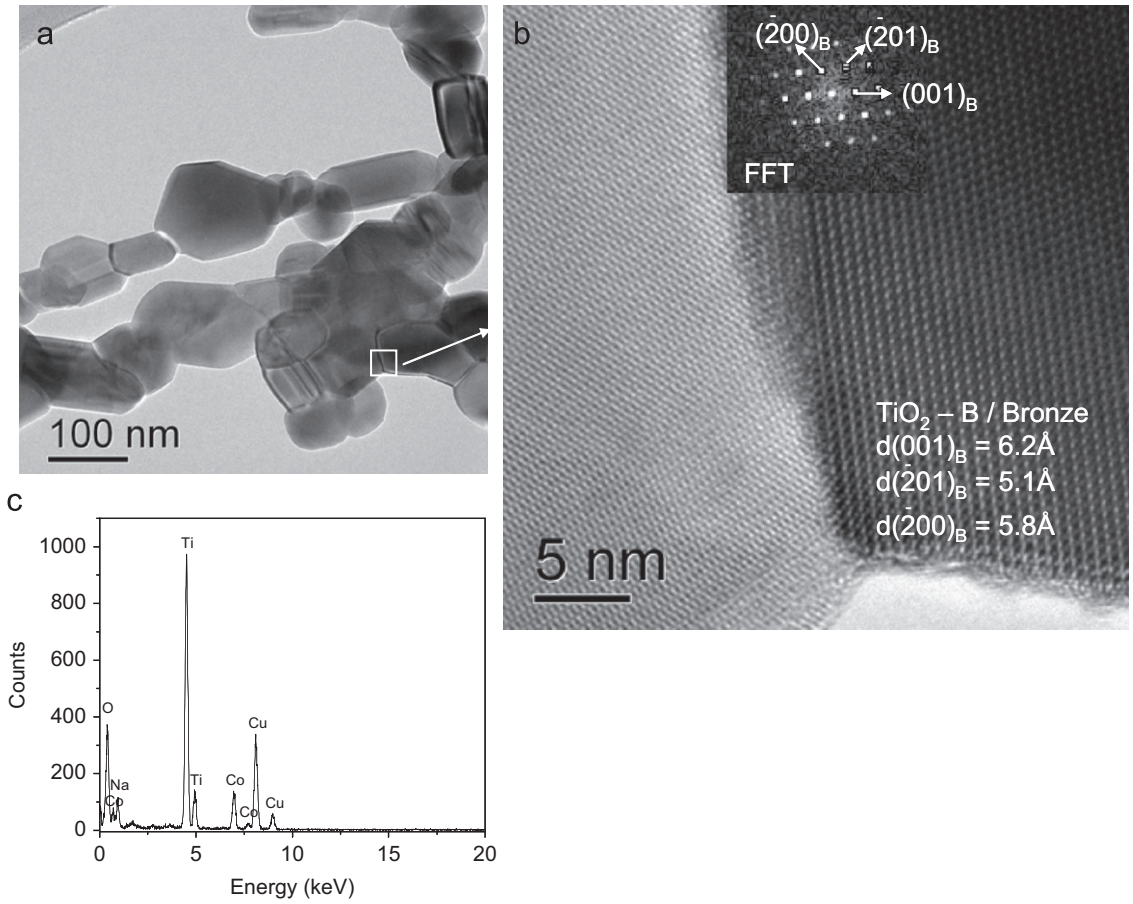


**Fig. 10.** TEM images of sample Co-TTNS/30 heat-treated at 800 °C: (a) lower magnification, (b) HRTEM of a $TiO_2$–B crystal with the fast Fourier transform of the image as an inset and (c) the corresponding EDS spectrum.

## Acknowledgments

The authors are grateful to PETROBRAS S.A. for financial support during realization of this work. The authors thank Andrea Pinheiro and Angelica Marques from SENAI/CTGas for the XRD and TG analyses and Dayse Lovatte and Denise Costa from CENPES for the DRS-UV–Vis and $N_2$ adsorption measurements.

## Appendix A. Supplementary data

Supplementary data associated with this article can be found in the online version at 10.1016/j.jssc.2008.10.008.

## References

[1] T. Kasuga, M. Hiramatsu, A. Hoson, T. Sekino, K. Niihara, Langmuir 14 (1998) 3160.
[2] J. Yang, D. Li, X. Wang, X. Yang, L. Lu, J. Mater. Sci. 38 (2003) 2907.
[3] S. Papp, L. Korosi, V. Meynen, P. Cool, E.F. Vansant, I. Dekany, J. Solid State Chem. 178 (2005) 1614.
[4] E. Morgado Jr., M.A.S. Abreu, O.R.C. Pravia, B.A. Marinkovic, P.M. Jardim, F.C. Rizzo, A.S. Araujo, Sol. State Sci. 8 (2006) 888.
[5] E. Morgado Jr., M.A.S. Abreu, G.T. Moure, B.A. Marinkovic, P.M. Jardim, A.S. Araujo, Chem. Mater. 19 (2007) 665.
[6] X. Sun, Y. Li, Chem. Eur. J. 9 (2003) 2229.
[7] R. Ma, T. Sasaki, Y. Bando, Chem. Commun. (2005) 948.
[8] B.A. Marinkovic, P.M. Jardim, E. Morgado Jr., M.A. Abreu, G.T. Moure, F. Rizzo, Mater. Res. Bull. 43 (2008) 1562.
[9] O.P. Ferreira, A.G. Souza, F. Mendes Filho, O.L. Alves, J. Braz. Chem. Soc. 17 (2) (2006) 393.
[10] X. Ding, X.G. Xu, Q. Chen, L.-M. Peng, Nanotechnology 17 (2006) 5432.
[11] D.V. Bavykin, A.A. Lapkin, P.K. Plucinski, L. Torrente-Murciano, J.M. Friedrich, F.C. Walsh, Top. Catal. 39 (3–4) (2006) 151.
[12] E. Morgado Jr., P.M. Jardim, B.A. Marinkovic, F.C. Rizzo, M.A.S. Abreu, J.L. Zotin, A.S. Araujo, Nanotechnology 18 (2007) 495710.
[13] D. Wu, Y. Chen, J. Liu, X. Zhao, A. Li, N. Ming, Appl. Phys. Lett. 87 (2005) 112501.
[14] C. Huang, X. Liu, L. Kong, W. Lan, Q. Su, Y. Wang, Appl. Phys. A 87 (2007) 781.
[15] X.G. Xu, X. Ding, Q. Chen, L.-M. Peng, Phys. Rev. B 73 (2006) 165403.
[16] M.A. Debeila, E. Raphulu, E. Mokoena, M. Avalos, V. Petranovski, N.J. Coville, M.S. Scurrel, Mater. Sci. Eng. A 396 (2005) 70.
[17] S.J. Gregg, K.S.W. Sing, Adsorption, Surface Area, and Porosity, second ed., Academic Press, London, 1982;
S. Lowell, J.E. Shields, M.A. Thomas, M. Thommes, Characterization of Porous Solids and Powders: Surface Area, Pore Size, and Density, Kluwer Academic Publishers, Dordrecht, The Netherlands, 2004.
[18] E. Morgado Jr., M.A.S. Abreu, G.T. Moure, B.A. Marinkovic, P.M. Jardim, A.S. Araujo, Mater. Res. Bull. 42 (2007) 1748.
[19] D.V. Bavykin, J.M. Friedrich, F.C. Walsh, Adv. Mater. 18 (2006) 2807.
[20] H.G. Yang, H.C. Zhang, J. Am. Chem. Soc. 127 (2005) 270.
[21] H. Zhu, Y. Lan, X. Gao, S.P. Ringer, Z.F. Zheng, J. Zhao, J. Am. Chem. Soc. 127 (2005) 6730.
[22] D.V. Bavykin, J.M. Friedrich, A.A. Lapkin, F.C. Walsh, Chem. Mater. 18 (2006) 1124.
[23] C.-C. Tsai, H. Teng, Chem. Mater. 18 (2006) 367.
[24] L. Pauling, The Nature of the Chemical Bond, third ed., Cornell University Press, Ithaca, NY, 1960.
[25] M. Ampo, H. Yamashita, Fine Chem. 25 (1996) 39.
[26] T. Nishikawa, T. Nakajima, Y. Shinohara, J. Mol. Struct. (Theochem.) 545 (2001) 67.
[27] C. Wang, D.W. Behnemann, J.K. Dohrmann, Chem. Commun. (2000) 1539.
[28] R. Asahi, T. Morikawa, T. Ohwaki, K. Aoki, Y. Taga, Science 293 (2001) 269.
[29] G. Wu, T. Nishikawa, B. Ohtani, A. Chen, Chem. Mater. 19 (2007) 4530.
[30] W. Choi, A. Termin, R.M. Hoffmann, J. Phys. Chem. 98 (1994) 13669.
[31] S. Singh, N. Rama, M.S. Ramachandra Rao, Appl. Phys. Lett. 88 (2006) 222111.
[32] R. Marchand, L. Brohan, M. Tournoux, Mater. Res. Bull. 15 (1980) 1129.